Crystal-Like Rearrangements of Icosahedra in Simulated Copper-Zirconium Metallic Glasses and their Effect on Mechanical Properties

J. Zemp,[1] M. Celino,[2] B. Schönfeld,[1] and J. F. Löffler[1,*]
[1]Laboratory of Metal Physics and Technology, Department of Materials, ETH Zurich, 8093 Zurich, Switzerland
[2]ENEA, Italian National Agency for New Technologies, Energy and Sustainable Economic Development, C.R. Casaccia, Via Anguillarese 301, 00123 Rome, Italy
(Received 19 March 2015; published 13 October 2015)

Indications of the Cu_2Zr Laves phase are observed in MD simulations of amorphous $Cu_{64}Zr_{36}$ upon isothermal holding just above the glass transition temperature. The structural evolution towards Cu_2Zr is accompanied by an increase in the fraction of Cu-centered icosahedra, which demonstrates that a large icosahedral fraction does not just indicate structural relaxation. The crystal-like regions generate an increase in strength and Young's modulus, and a stronger localized shear band. A universal relation between the fraction of full icosahedra and their interconnectivity is found, and both can be modified simultaneously via changes of temperature or strain.

DOI: 10.1103/PhysRevLett.115.165501 PACS numbers: 61.43.Bn, 62.23.Pq, 62.25.Mn, 81.05.Kf

The structure of glasses and liquids is a fundamental topic in condensed matter physics and much less understood than the structure of crystalline materials. The polytetrahedral packing model [1] suggests that icosahedra are a basic structural unit which competes directly with the formation of face-centered cubic or hexagonal close-packed structures. Because of their fivefold symmetry, icosahedra are incompatible with long-range translational order and are thus often found in glasses and quasicrystals. Icosahedral short-range order (SRO) is observed in a variety of metallic glasses (MGs) [2,3] and according to Frank's hypothesis [4] provides a barrier against crystallization, at least in pure metals. Understanding the structure of MGs and especially the role of icosahedra with respect to glass formation and thermal stability is a central question in the field of MGs, and that of amorphous materials in general.

The arrangement of icosahedra into a three-dimensional space-filling structure can be conceptually understood by the efficient cluster packing model [5]. The distribution of icosahedra in Cu-Zr-based MGs, however, suggests the formation of string- or network-like icosahedral superclusters [6–9]. Besides the importance of icosahedra in MGs, crystalline structures such as the $MgZn_2$-type Laves phase also comprise icosahedral clusters. In fact, many bulk MGs are found near Laves phases [10]. Tang and Harrowell [11] have also shown that for Mendelev's interaction potential [12] the Cu_2Zr Laves phase possesses a lower energy than $Cu_{10}Zr_7$, which is reported to be the stable structure at room temperature in the experimental phase diagram [13]. Furthermore, based on differential thermal analysis data, a Cu_2Zr phase was introduced in Ref. [14] and its existence was also addressed in Refs. [13,15,16]. Computer simulations of Cu-Zr MGs have indicated the importance of Cu-centered icosahedra, whose number significantly increases during cooling [6–8,17,18] and isothermal holding [9,19]. With the Laves phase as the candidate for the primary crystallization phase, a large number of icosahedra may, however, simply indicate crystallization.

A major goal of structural investigations of MGs is to link their structure to the mechanical properties. MGs usually show very limited plastic deformation, which is localized in a thin region called shear band (SB) that is characterized by pronounced changes in the atomic structure [20,21]. An increasing number of icosahedra generates an increase in strength but also reduces plasticity [7]. On the other hand, introducing heterogeneities such as finely dispersed nano- or micrometer-sized crystals can enhance plasticity [22–24]. The introduction of Cu precipitates into $Cu_{64}Zr_{36}$ was studied by Albe *et al.* [25]: they found a decrease in strength and less localized SB formation, indicating more plastic behavior. The effect of nanocrystals on mechanical properties, however, depends on their structure, shape, and size [26]. Any crystallization that occurs in the course of molecular dynamics (MD) simulations is expected to affect the mechanical properties of the sample.

In this Letter, we investigate the role of icosahedral SRO in MGs. For this we have simulated binary Cu-Zr and show that crystallization occurs towards a Laves phase (here Cu_2Zr). This agrees well with experimental work on Cu-Zr-Ti [27] or the Zr-based bulk MG Vit 1 [28], where the primary forming crystals are indeed Laves phases. The presence of these crystallites is shown to influence the mechanical properties of MGs. Thus we analyze here the distribution and interconnectivity of icosahedra within and outside the SB. We find that the SB undergoes a stress-induced glass transition upon deformation, which supports recent experimental [29] and simulation [30] results.

The semiempirical potential by Mendelev *et al.* [12] was used to simulate $Cu_{64}Zr_{36}$ in LAMMPS [31] using the NPT ensemble at zero pressure. A sample (referred to as the "annealed sample") containing 11 664 atoms (about $57 \times 57 \times 57$ Å^3) was produced by cooling with a rate of 0.01 K/ps from 2000 to 800 K, held at 800 K for 300 ns (termed "annealing"), and finally cooled to 50 K with the same rate of 0.01 K/ps. A second sample (referred to as the "as-cast sample") was produced in the same way, but the annealing for 300 ns at 800 K was omitted. The nearest-neighbor distances and coordination numbers obtained agree well with the data of Ref. [12]. To observe shear localization, large samples were built from $2 \times 4 \times 8$ replicas of the as-cast and annealed samples. Periodic boundary conditions were used in the z and x direction together with free surfaces in the y direction. The effect of different boundary conditions is discussed in Ref. [32]. An annealing step at 800 K for 2 ns followed by cooling down to 50 K at a cooling rate of 0.1 K/ps was applied to relax the surfaces. The samples were then deformed in compression along the z axis at a constant deformation rate of 10^7 s^{-1}. At a strain of about 15% the stress in the loading direction was removed and the inherent structure [33] was determined; i.e., any atomic displacement due to thermal vibrations was removed by relaxing the atoms into their potential energy minimum using the conjugate gradient method. To identify shear localization the local atomic shear strain η_{Mises} [34] was calculated.

The topological SRO was determined by the Voronoi tessellation method. The Voronoi index (VI) is denoted as $\langle n_3 n_4 n_5 n_6 \rangle$ with n_i as the number of i-edged polygons. Full icosahedra (FI) have a VI of $\langle 0\,0\,12\,0 \rangle$ and may form superclusters by cap-sharing bonds, which occur when a shell atom of a FI is again the center of another FI. Among the types of bonds between FI (vertex-, edge-, face-, and cap-sharing), cap-sharing bonds are of special interest because of their lowest potential energy [7]. The number of cap-sharing bonds per FI, n, is used as a measure for interconnectivity [6,8,9].

Figure 1(a) shows a slice (1 nm in thickness) of the annealed sample. Interestingly, crystal-like regions with sixfold symmetry, as known for the Cu_2Zr Laves phase, can be observed. The structural similarity between Cu_2Zr and the crystal-like regions is illustrated as Fig. S1 in the Supplemental Material [35]. These regions grow larger with extended annealing, as shown in Fig. S2. The lattice parameters, as determined from the projection of the atomic positions along the individual axis, are $a = 5.10(2)$ and $c = 8.28(4)$ Å, which agrees well with data from previous simulations of the Cu_2Zr Laves phase [11] and with experimental data of the structurally similar Cu_2ZrTi [36]. The Cu_2Zr Laves phase is made up entirely from Cu-centered Cu_7Zr_6 FI with an interconnectivity of $n = 6$ and Zr-centered CN16 Frank-Kasper polyhedra (with a VI of $\langle 0\,0\,12\,4 \rangle$). A similar increase of these two cluster types during annealing was also observed using the simulation potential by Cheng *et al.* [18,19]. However, while these authors attributed that finding to structural relaxation, we clearly find early stages of crystallization upon annealing, where the fraction of Cu atoms in the center of Cu_7Zr_6 icosahedra with $n = 6$ is about 2%. The size of the crystal-like regions is just a few nanometers, and thus the number of Cu atoms at the crystalline-amorphous interface is large. Figure 1(b) shows solely the center atoms of FI, colored according to their interconnectivity n. One observes that besides atoms with $n = 6$, atoms with $n = 5$ and $n = 4$ also show sixfold symmetry, whereas atoms with $n < 4$ occupy the space between the crystal-like regions. Thus, these results provide the first demonstration for an onset of crystallization in MD-simulated $Cu_{64}Zr_{36}$. However, while the presence of a Cu_2Zr phase has been addressed in Refs. [13–16], the existence of the Cu_2Zr Laves phase in stable or metastable form should still be verified experimentally by scattering or imaging methods.

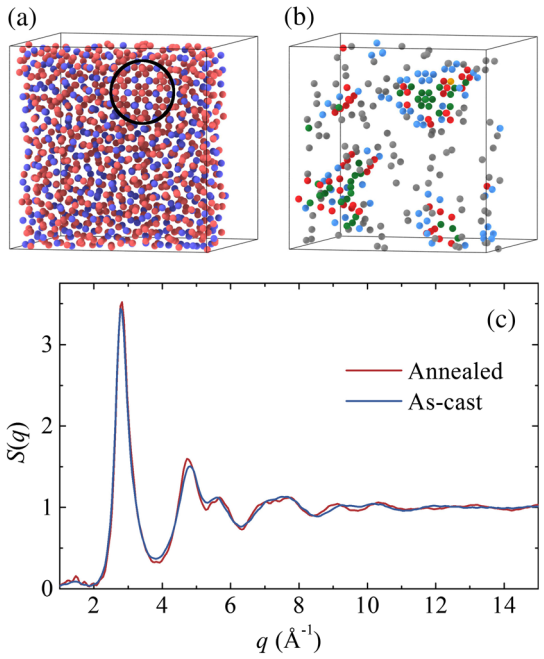

FIG. 1 (color online). (a) Slice of 1 nm thickness (Cu: red; Zr: blue) of the annealed sample. A crystal-like region oriented with its c axis along the viewing direction is seen (black encircled), revealing the sixfold symmetry of the Cu_2Zr Laves phase. Similar regions can be visually identified by tilting the sample box and adjusting the slice thickness. (b) The same atomic configuration, where only FI-center atoms are shown, colored according to their interconnectivity n (<4: gray, 4: blue, 5: red, 6: green, 7: yellow). Atoms with high interconnectivity are arranged in crystal-like regions while atoms with $n < 4$ occupy the space in between. (c) Total neutron structure factor $S(q)$ for the as-cast (blue) and annealed (red) samples at 50 K.

Figure 1(c) shows for the as-cast and annealed samples the Faber-Ziman neutron structure factors [37] from the simulated inherent atomic configurations at 50 K, calculated by Fourier transformation of the partial pair correlation functions $g_{ij}(r)$:

$$S_{ij}(q) = 1 + 4\pi\rho \int r^2[g_{ij}(r) - 1]\frac{\sin qr}{qr}dr,$$

where q is the magnitude of the scattering vector, ρ is the atomic density, and r is the interatomic distance. The total structure factor is the weighted sum of the partial structure factors

$$S(q) = \sum_{i,j} x_i x_j \frac{b_i b_j}{\langle b \rangle^2} S_{ij}(q),$$

where x_i represents the atomic fractions and b_i the coherent scattering lengths with neutrons. The structure factor of the annealed sample shows additional features compared to that of the as-cast sample, which suggests the presence of better defined local atomic arrangements. The overall appearance, however, still resembles an amorphous structure rather than a crystal. It should be kept in mind that the experimental (and similarly the noninherent) structure factor will be smeared due to thermal displacements, which are absent in the inherent structure.

Figure 2 shows the stress-strain curves for the as-cast and annealed samples together with the atomic configurations following deformation. Atoms in (b) and (c) are colored according to their local atomic shear strain. As can be seen in Fig. 2(a), the annealed sample shows greater stiffness and greater yield strength than the as-cast sample. After yielding, a sharp stress drop is observed in the annealed sample, whereas a smoother transition is seen in the as-cast sample. The flow stress, however, is comparable in both samples, which means that the shear resistance of the SBs is similar.

Nanocrystals can have different effects on strength and plasticity in bulk MGs [22]. For example, in Ref. [25] the presence of Cu precipitates in $Cu_{64}Zr_{36}$ led to the formation of multiple SBs, whereas Figs. 2(b) and 2(c) show only a single SB. The crystalline-amorphous interface may act as a SB nucleation site due to the structural mismatch between the crystalline and amorphous phases, which reduces the strength but improves plasticity [38]. While for most crystals the structure differs greatly from the amorphous structure, the SRO of the Cu_2Zr Laves phase is very similar to that of the amorphous matrix so that here the interface is not expected to significantly facilitate SB formation. The Cu precipitates in Ref. [25] show also dislocation activity and stay crystalline during deformation, whereas the crystal-like regions in this work become amorphized, as shown in the insets to Fig. 2(a). This agrees with recent findings which show that for crystallite dimensions below a certain threshold, deformation generates the dissolution of crystalline inclusions and, consequently, glass-like plasticity [26]. The crystal-like regions are presumably too small to influence SB activity. In addition, Laves phases are brittle and thus the required energy for dislocation activity is higher for the Laves phase than for face-centered cubic [25] or hexagonal close-packed [26] inclusions.

Figure 3 shows the FI fraction, local atomic shear strain, and interconnectivity as a function of distance from the lateral center of the SB. While the FI fraction in the matrix of the as-cast and annealed samples differs greatly, it is comparable in the SB region, which is characterized by a peak in the local atomic shear strain. The larger FI fraction in the annealed sample generates an increase in the elastic modulus and strength of annealed Cu-Zr metallic glasses [see Fig. 2(a)] compared to the as-cast state. The same type of relation between FI fraction and mechanical properties has also been observed in Ref. [7]. Thus, it takes more stress to deteriorate the bulk structure of the annealed sample, which leads to greater strain localization, i.e., to a thinner SB. The stronger shear localization in the annealed sample can be observed clearly by comparing Figs. 2(b) and 2(c).

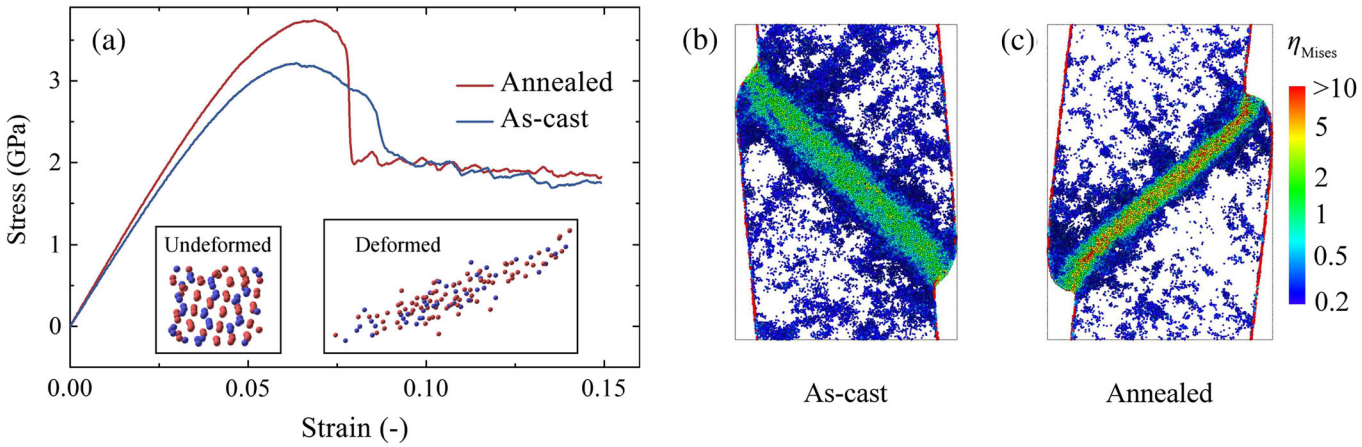

FIG. 2 (color online). (a) Stress-strain curves of the as-cast (blue) and annealed (red) states. A larger Young's modulus and greater yield strength are observed for the annealed sample. The insets show a selected crystal-like region (Cu: red; Zr: blue) within the SB region before and after deformation. (b),(c) SBs in as-cast and annealed $Cu_{64}Zr_{36}$ after deformation and unloading. Atoms are colored according to their local atomic shear strain η_{Mises} (logarithmic scale) and only atoms with a local strain greater than 0.2 are shown. In the annealed state the strain is more strongly localized in the SB and less strain is carried by the matrix.

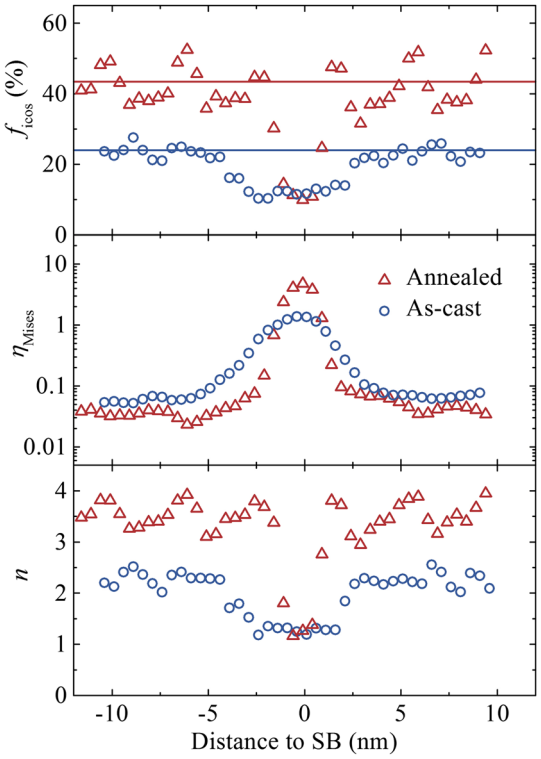

FIG. 3 (color online). FI fraction f_{icos}, local atomic shear strain η_{Mises}, and interconnectivity n as a function of the distance from the lateral center of the SB for the as-cast (blue) and annealed (red) samples. The solid horizontal lines in the upper image represent the average FI fractions for the undeformed bulk samples. The SBs are characterized by a low FI fraction, large local strain, and low interconnectivity.

The interconnectivity among FI is directly linked to the FI fraction, irrespective of thermal history or temperature. Figure 4 shows the data from Fig. 3 together with data from undeformed samples at different temperatures and after different thermal treatments [9]. Because of crystallization, which limits interconnectivity to a maximum of $n = 6$, the slope of the curve decreases with increasing FI fraction. Surprisingly, the relation of FI fraction and interconnectivity due to mechanical deformation is similar to that obtained from the data of the undeformed samples; i.e., all data collapse on a universal curve. In the undeformed samples low FI fractions and low interconnectivity represent the structure at high temperatures [9], while the FI fraction in the SBs is also low at 50 K (~10%) with an interconnectivity of ~1.2. Thus, the FI fraction within the deformed SB at 50 K is comparable to that in the undeformed bulk sample at a temperature between 840 and 880 K. The structural changes due to mechanical deformation are similar to those obtained at temperatures in the supercooled liquid region, i.e., the region between the glass transition temperature $T_g \approx 745$ K (experimental value) and the liquidus temperature $T_l \approx 1230$ K, and can thus be understood to be the result of a stress-induced glass transition. A similar conclusion was drawn by Guan *et al.* [30] by evaluating the steady-state flow stress, and also by Klaumünzer *et al.* [29], who experimentally determined an equivalent temperature from values of SB dilation within the SB initiation stage. It should be emphasized that Fig. 4 represents a universal curve, where the relation between FI fraction and interconnectivity is fixed; i.e., both can only be modified simultaneously. Both decrease, for example, simultaneously at higher strain or higher temperature.

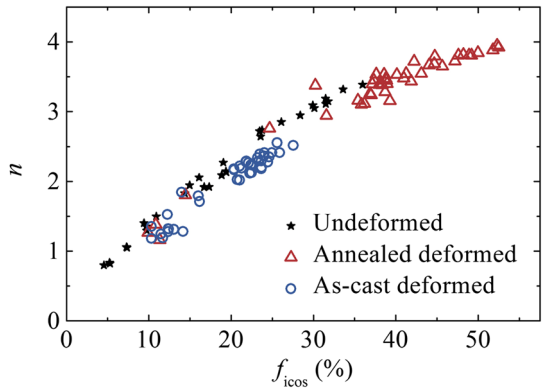

FIG. 4 (color online). Average interconnectivity n as a function of FI fraction for deformed as-cast (blue) and annealed (red) samples at 50 K. The undeformed data are taken from Ref. [9] and represent states at different temperatures and after different thermal treatments. All data collapse on a universal curve.

In summary, MD simulation shows early stages of crystallization in amorphous $Cu_{64}Zr_{36}$ upon annealing above T_g, where the primary crystallization phase is the Cu_2Zr Laves phase, made up of Cu-centered icosahedra and Zr-centered CN16 Frank-Kasper polyhedra. The increase in icosahedral fraction during annealing is therefore due to crystallization and not only, as previously thought, due to structural relaxation. Thus the good glass-forming ability of Cu-Zr-based MGs does not necessarily result from a high icosahedral fraction. As to mechanical properties, the formation of crystal-like regions upon annealing generates an increase in strength and Young's modulus, and a narrower SB. Because of the structural similarity of the Cu_2Zr Laves phase to the $Cu_{64}Zr_{36}$ glass, SB initiation is largely suppressed, such that plastic deformation still proceeds via one major shear band. The destruction of the icosahedral network in the SB region can be identified as resulting from a stress-induced glass transition, which contributes to the further understanding of glass deformation.

Support by the Swiss National Science Foundation (SNF Grant No. 200020-153103) is gratefully acknowledged. The computations were performed using resources provided by the CRESCO–ENEA GRID High Performance Computing infrastructure.

*joerg.loeffler@mat.ethz.ch

[1] D. R. Nelson and F. Spaepen, Solid State Phys. **42**, 1 (1989).
[2] A. C. Y. Liu, M. J. Neish, G. Stokol, G. A. Buckley, L. A. Smillie, M. D. de Jonge, R. T. Ott, M. J. Kramer, and L. Bourgeois, Phys. Rev. Lett. **110**, 205505 (2013).
[3] W. K. Luo, H. W. Sheng, F. M. Alamgir, J. M. Bai, J. H. He, and E. Ma, Phys. Rev. Lett. **92**, 145502 (2004).
[4] F. C. Frank, Proc. R. Soc. A **215**, 43 (1952).
[5] D. B. Miracle, Nat. Mater. **3**, 697 (2004).
[6] M. Wakeda and Y. Shibutani, Acta Mater. **58**, 3963 (2010).
[7] M. Lee, C.-M. Lee, K.-R. Lee, E. Ma, and J.-C. Lee, Acta Mater. **59**, 159 (2011).
[8] R. Soklaski, Z. Nussinov, Z. Markow, K. F. Kelton, and L. Yang, Phys. Rev. B **87**, 184203 (2013).
[9] J. Zemp, M. Celino, B. Schönfeld, and J. F. Löffler, Phys. Rev. B **90**, 144108 (2014).
[10] H. J. Fecht and W. L. Johnson, Mater. Sci. Eng. A **375–377**, 2 (2004).
[11] C. Tang and P. Harrowell, J. Phys. Condens. Matter **24**, 245102 (2012).
[12] M. I. Mendelev, M. J. Kramer, R. T. Ott, D. J. Sordelet, D. Yagodin, and P. Popel, Philos. Mag. **89**, 967 (2009).
[13] D. Arias and J. P. Abriata, J. Phase Equilib. **11**, 452 (1990).
[14] E. Kneller, Y. Khan, and U. Gorres, Z. Metallkd. **77**, 43 (1986).
[15] M. H. Braga, L. F. Malheiros, F. Castro, and D. Soares, Z. Metallkd. **89**, 541 (1998).
[16] N. Wang, C. Li, Z. Du, F. Wang, and W. Zhang, CALPHAD: Comput. Coupling Phase Diagrams Thermochem. **30**, 461 (2006).
[17] Y. Q. Cheng, H. W. Sheng, and E. Ma, Phys. Rev. B **78**, 014207 (2008).
[18] Y. Q. Cheng, E. Ma, and H. W. Sheng, Phys. Rev. Lett. **102**, 245501 (2009).
[19] J. Ding, Y.-Q. Cheng, and E. Ma, Acta Mater. **69**, 343 (2014).
[20] Y. Ritter and K. Albe, Acta Mater. **59**, 7082 (2011).
[21] R. Maaß and J. F. Löffler, Adv. Funct. Mater. **25**, 2353 (2015).
[22] J. Eckert, J. Das, S. Pauly, and C. Duhamel, J. Mater. Res. **22**, 285 (2007).
[23] M. Calin, J. Eckert, and L. Schultz, Scr. Mater. **48**, 653 (2003).
[24] K. Hajlaoui, A. R. Yavari, A. LeMoulec, W. J. Botta, F. G. Vaughan, J. Das, A. L. Greer, and Å. Kvick, J. Non-Cryst. Solids **353**, 327 (2007).
[25] K. Albe, Y. Ritter, and D. Şopu, Mech. Mater. **67**, 94 (2013).
[26] A. C. Lund and C. A. Schuh, Philos. Mag. Lett. **87**, 603 (2007).
[27] H. Men, S. J. Pang, and T. Zhang, Mater. Sci. Eng. A **408**, 326 (2005).
[28] C. C. Hays, C. P. Kim, and W. L. Johnson, Appl. Phys. Lett. **75**, 1089 (1999).
[29] D. Klaumünzer, A. Lazarev, R. Maaß, F. H. Dalla Torre, A. Vinogradov, and J. F. Löffler, Phys. Rev. Lett. **107**, 185502 (2011).
[30] P. Guan, M. Chen, and T. Egami, Phys. Rev. Lett. **104**, 205701 (2010).
[31] S. Plimpton, J. Comput. Phys. **117**, 1 (1995).
[32] Y. Ritter, PhD thesis, TU Darmstadt, 2012.
[33] F. H. Stillinger and T. A. Weber, Phys. Rev. A **25**, 978 (1982).
[34] F. Shimizu, S. Ogata, and J. Li, Mater. Trans., JIM **48**, 2923 (2007).
[35] See Supplemental Material at http://link.aps.org/supplemental/10.1103/PhysRevLett.115.165501 for more information on structural aspects.
[36] J. Z. Jiang, H. Kato, T. Ohsuna, J. Saida, A. Inoue, K. Saksl, H. Franz, and K. Ståhl, Appl. Phys. Lett. **83**, 3299 (2003).
[37] T. E. Faber and J. M. Ziman, Philos. Mag. **11**, 153 (1965).
[38] Y. Shi and M. L. Falk, Acta Mater. **56**, 995 (2008).